Long-range antiferromagnetic order in malonate-based compounds Na2M(H2C3O4)2×2H2O (M = Mn, Fe, Co, Ni)

Gwenaelle Rousse, G. Radtke, Y. Klein, H. Ahouari

Long-range antiferromagnetic order in malonate-based compounds $Na_2M(H_2C_3O_4)_2{\cdot}2H_2O$ (M=Mn, Fe, Co, Ni)

G. Rousse,[a,b,c,*] G. Radtke,[c] Y. Klein,[c] and H. Ahouari[d,e]

[a]FRE 3677, Chimie du Solide et de l'Energie, Collège de France, 11 place Marcelin Berthelot, 75231 Paris Cedex 05, France

[b]Réseau sur le Stockage Electrochimique de l'Energie (RS2E), FR CNRS 3459, France

[c]Institut de Minéralogie, de Physique des Matériaux, et de Cosmochimie (IMPMC), Sorbonne Universités - UPMC Univ Paris 06, UMR CNRS 7590, Muséum National d'Histoire Naturelle, IRD UMR 206, 4 place Jussieu, F-75005 Paris, France.

[d]Laboratoire de Réactivité et Chimie des Solides, UMR CNRS 7314, 33 Rue Saint Leu 80039 Amiens Cedex.

[e]ALISTORE-European Research Institute, FR CNRS 3104, 80039 Amiens, France

*Email: gwenaelle.rousse@college-de-france.fr

Abstract

The recently discovered metal-malonate compounds of formulae $Na_2M(H_2C_3O_4)_2{\cdot}2H_2O$ with M=Mn, Fe, Co, Ni are investigated for their magnetic properties. While the Cu-based material is a weak ferromagnet, all other members present antiferromagnetic interactions. Neutron powder diffraction experiments reveal the establishment of a long range magnetic order at low temperature in the *Pbca* Shubnikov magnetic group. The magnetic structures are characterized by antiferromagnetic layers perpendicular to [001]. These layers are stacked antiparallel (M=Fe) or parallel (M=Mn, Ni) in the (a, c) plane. Magnetic moments are collinear to **b** for the former and to **c** for the latter. The M=Co malonate exhibits a non-collinear magnetic structure intermediate between the two latter, with components along **b** and **c.** Density functional theory calculations indicate that the dominant magnetic interaction, J_1, occurs along a malonate group via a carboxylate and links two transition metals within the same layer, while other interactions (inter- or intra- layer) are much weaker, so that these compounds present the dominant characteristics of 2D-antiferromagnets.

Introduction

Transition metal (TM) molecular based compounds have been studied for years because they present many useful properties such as catalytic activity, electric conductivity, non-linear optical properties… The choice of the organic ligand determines the network topology and therefore the functionalities of a material.[1–4] Moreover, a given TM-ligand pair can lead to a wide variety of compounds thanks to the many possible coordination modes and to the flexibility of the ligand. Among carboxylate ligands, many synthesis efforts have led to the discovery of new functional materials with the formate, oxalate, terephthalate, maleate, and malonate groups.[5–9] When coupled with a *3d* transition metal, these ligands may induce interesting functionalities. Among them, one can cite peculiar magnetic behaviors e.g. (anti)ferromagnetism, magnetoelectricity and multiferroicity.[7,10–12] Carboxylates are versatile ligands that can chelate a TM in different bridging modes: *syn-syn*, *syn-anti*, and *anti-anti*, through one or both carboxylate groups.[12,13] Moreover, it has been shown that malonates can mediate significant ferromagnetic or antiferromagnetic interactions between TM.[5,8,9,14–19]
While the macroscopic magnetic properties exploration of TM molecular based compounds are routine, magnetic structure determination from neutron diffraction has been sporadic, because the distance between two transition metal ions can be fairly large and may prevent long-range ordering. Moreover, these ligands often present many hydrogen atoms which create diffuse scattering, making neutron diffraction experiments and their analysis more difficult; the use of deuterated ligands is indeed not always possible. Therefore, only few reports can be found in literature about the establishment and determination of magnetic structures mediated by organic ligands.[10,20–22]

In this paper, we explore the magnetic behavior and magnetic structures of a recently discovered metal-malonate family of formulae $[Na_2(\mu\text{-}H_2O)_2M(C_3H_2O_4)_2]_n$ - denoted thereafter $Na_2M(H_2C_3O_4)_2{\cdot}2H_2O$ for sake of simplicity- where *M* is a transition metal at the 2+ oxidation state. $Na_2Cu(H_2C_3O_4)_2{\cdot}2H_2O$ was first reported in 2005 by Ghoshal et al.[23] Besides solving the crystal structure from single crystal X-Ray diffraction, they studied its magnetic behavior, concluding that it exhibits weak ferromagnetic interactions with, however, no long range ordering. We recently extended the family of these malonates by synthetizing $Na_2M(H_2C_3O_4)_2{\cdot}2H_2O$ with *M*=Mn, Fe, Co and Ni and showed that some of them might be interesting as Li-ion battery electrode compounds.[24] In this paper, we demonstrate that they

order antiferromagnetically in different magnetic structures depending on the nature of *M*. Moreover, we use density functional theory (DFT) calculations to estimate exchange interactions between magnetic ions.

Experimental and computational details

X-ray and neutron Diffraction: XRD patterns of the as-prepared compounds were recorded using either a Bruker D8-Advance Diffractometer with Cu-K_α radiation (λ_1= 1.54056 Å, λ_2= 1.54439 Å) equipped with a LynxEye detector operating at 40 kV and 40 mA.
Complementary Synchrotron X-Ray patterns were recorded at the 11-BM beamline at Argonne National Lab. The finely ground powder was loaded in a 0.5 mm diameter capillary and the sample was measured in transmission mode (λ=0.4138 Å).
Neutron patterns were recorded as a function of temperature on the G41 high flux powder diffractometer of Orphée reactor at Laboratoire Léon Brillouin, Saclay, France. The powdered samples were placed in a vanadium cylindrical container (diameter 8 mm). A wavelength of 2.423 Å obtained from a graphite monochromator was used.
All powder patterns were refined using the Rietveld method[25] as implemented in the FullProf program.[26]

Magnetic measurements: Temperature-dependent susceptibility measurements were carried out using a SQUID (Quantum design), in zero field cooled (ZFC) and field cooled (FC) modes, under an applied magnetic field of 5 kOe or 10 kOe. 20-30 mg of powder was placed into gel caps for the measurement. Magnetization curves M= f(H) were recorded at 5 K on a Physical Property Measurement System (PPMS) from Quantum Design equipped with a Vibrating Sample Magnetometer.

Calculations: Calculations were carried out using QUANTUM ESPRESSO[27]. This suite of codes is based on DFT and uses the pseudopotential plane-wave method. Ultrasoft pseudopotentials[28] have been employed with plane-wave and charge density cutoffs of, respectively, 60 and 400 Ry. GGA-PBE[29] has been used for exchange and correlation, augmented by a Hubbard U term to improve the treatment of strongly correlated transition metal *3d* electrons. A value of the effective self-consistent Hubbard U was determined following the approach described in refs.30,31 in a 108-atom orthorhombic cell, using the experimental structure determined at 1.5 K. Values of U_{scf} = 5.75, 5.85, 6.25 and 10.50 eV

have been obtained for Mn, Co, Ni and Cu, respectively. The experimental atomic positions have been subsequently optimized in GGA+U_{scf} prior to the calculation of magnetic couplings. This structural optimization was performed to determine accurately hydrogen positions, starting from the models obtained from the refinement of neutron powder diffraction data. At the end the relaxation procedure, atomic forces were less than 10^{-4} Ry/bohr. Calculations have been carried out on the full series of malonates except for Fe, as accurate structural data are lacking in this case. As subtle effects associated with orbital degeneracy for HS Fe^{2+} in octahedral field might be expected, a precise knowledge of the experimental crystal structure is indeed mandatory in such a case.

The computation of isotropic magnetic couplings was carried out within the broken symmetry formalism, i.e. by mapping total energies corresponding to various collinear spin arrangements within a supercell onto a Heisenberg Hamiltonian

$$\widehat{H} = \widehat{H}_0 + \sum_{i>j} J_{ij}\, \hat{\mathbf{S}}_\mathbf{i} \cdot \hat{\mathbf{S}}_\mathbf{j}$$

Eq. 1

where $\widehat{H}_0$ is the spin-independent part of the Hamiltonian, J_{ij} are the magnetic couplings to determine and $\hat{\mathbf{S}}_\mathbf{i}$ and $\hat{\mathbf{S}}_\mathbf{j}$ the spin S operators localized on the transition metal sites i and j.

It is straightforward to show that the expectation value of this Hamiltonian on a DFT state $|\alpha\rangle$ (obtained by preparing the initial electron density according to a particular collinear spin arrangement in the supercell and performing a self-consistent calculation until convergence) can be simply written under the form of an Ising Hamiltonian[32]

$$\epsilon_\alpha^{DFT} = \langle\alpha|\widehat{H}|\alpha\rangle = \epsilon_0 + S^2 \sum_{i>j} J_{ij}\ \sigma_i\, \sigma_j$$

Eq. 2

where $\sigma_i = \pm 1$. In these malonates, the calculation of the magnetic couplings up to the fifth nearest-neighbors has been carried out in 216-atom cells obtained by doubling the orthorhombic unit cell either along the *a* (supercell A) or the *b* (supercell B) crystals axis. Classifying the magnetic couplings according to the metal-metal distance, as indicated in Figure 10, Equation 2 now reads

$$\epsilon_\alpha^{DFT,s} = \epsilon_0^s + \sum_{k=1}^{5} a_{\alpha,k}^s J_k$$

Eq. 3

where $s = A, B$ denotes the supercell and $a_{\alpha,k}^s$ are spin S, supercell and configuration dependent coefficients.

Taking crystal and spin reversal symmetries into account, a total of 22 inequivalent spin configurations of degeneracy g_α^s were obtained out of the $2^8 = 256$ possibilities in both cases. A numerical evaluation of the couplings is thus obtained through a least-squares minimization of the difference between DFT and Ising relative energies for these sets of spin configurations[33–35], i.e. by minimization of

$$F = \sum_{s=A,B} \sum_{\alpha=1}^{22} g_\alpha^s \left(\epsilon_\alpha^{DFT,s} - \epsilon_0^s - \sum_{k=1}^{5} a_{\alpha,k}^s J_k \right)^2$$

Eq. 4

Results

a) Preparation and structural characterization

Malonate compounds $Na_2M(H_2C_3O_4)_2{\cdot}2H_2O$ (*M*= Mn, Fe, Co, Ni, Cu) were synthetized as reported in refs 23,24. $MCl_2{\cdot}nH_2O$, $H_4C_3O_4$, $CH_3COONa{\cdot}3H_2O$ and NaCl precursors in a 1:3:6:14 molar ratio were dissolved in 6 ml of distilled water. The mixture was then heated to 100-150°C for 2.5 hours in a 23 ml capacity Teflon-lined autoclave followed by slow cooling to room temperature. The metal-malonate powders were recovered by rinsing with methanol to remove NaCl. Note that all phases are stable in air at room temperature, expect the Fe malonate which slowly decomposes (air aging).

The quality of the obtained Mn, Co and Ni powdered samples was confirmed from analysis of the synchrotron 11BM data recorded with λ= 0.4138 Å; NaCl was the only tiny impurity detected in the patterns of *M*=Mn, Co and Fe malonates, while the Ni-based one was pure. $Na_2Fe(H_2C_3O_4)_2{\cdot}2H_2O$ was found to suffer from degradation under the synchrotron beam,

explaining why its structure was refined against laboratory X-ray diffraction. Refinements were conducted in the orthorhombic space group *Pbca* starting from the model which was originally solved from single crystal diffraction,[23,24] and hydrogen atoms were not refined, apart for M=Mn (Hydrogen atoms were initially put at the value deduced from single crystal and then were freely refined). Final Rietveld refinements are shown in **Figure 1,** and **Table 1** gives the structural model refined for *M*=Mn. All compounds present basically the same structure, the main difference being the change in lattice parameters as a result of the different ionic size of 3*d* cations (**Table 1**).

The structure of the $Na_2M(H_2C_3O_4)_2{\cdot}2H_2O$ series of compounds is shown in **Figure 2** for *M*=Mn. The transition metal atom M sits in the middle of a slightly distorted octahedron built on oxygen atoms, each of them being part of a malonate group. Respectively, each malonate is linked in a bidentate way to the same *M* (via O1 and O2), and connects two adjacent *M* via O5 (**Figure 2d**). The fourth oxygen of the malonate group, O4, is not linked to *M* but points towards the hydrogen atoms of the water molecule (O3) so as to form an hydrogen bond, as discussed in our previous paper.[24] Finally, the carboxylate built on C3, O2 and O5 connects two M in an *anti-anti* bridging mode. Overall, this arrangement leads to a layered structure, with layers made of MO_6 octahedra and malonate groups stacked in the [001] direction (**Figures 2a,b**). A single layer is shown in **Figure 2c**. Na atoms and water molecules are located in the interlayer space.

The distance between metal-malonates layers being large (*c*/2, i.e. more than 8 Å), this family of compounds would in principle present much weaker inter-layer couplings compared to the intra-layer ones. However, the possible presence of long-range magnetic order cannot be ruled out on this sole consideration of large interatomic distances and motivated the study of the magnetic properties of this series of compounds.

b) Magnetization

The magnetic susceptibility of the 3*d*-metal malonate compounds $Na_2M(H_2C_3O_4)_2{\cdot}2H_2O$ (*M*=Mn, Fe, Co, Ni and Cu), summarized in **Figure 3**, can be fitted using the Curie-Weiss equation in the high temperature region (100-350 K):

$$\frac{1}{\chi} = \frac{T - \theta_{CW}}{C}$$

Eq. 5

Curie-Weiss temperatures (θ_{CW}) of -17 K, -23 K, -58 K and -60 K were obtained for the Mn, Fe, Co, and Ni, respectively. Negative values of θ_{CW} underline antiferromagnetic (AFM) interactions. Contrary to the latter cases, a positive value for the Cu-malonate, θ_{CW} ~ 1.6(1) K is found, in agreement with previous results by Ghoshal *et al.*, underlining very weak ferromagnetic (FM) interactions in this compound[23]. Effective moments extracted from the Curie constant are given in **Table 2**. The value for the Mn-malonate (5.95 μ_B) corresponds to the spin-only contribution of 5.92 μ_B expected for an isotropic d^5 cation in a regular octahedral environment.[36] The iron based and cobalt based compounds present effective moments of 5.29 μ_B and 5.22 μ_B respectively, i.e. higher than the 4.90 and 3.87 μ_B spin only contributions. This indicates a strong orbital contribution.[36] A small orbital contribution is also noticeable for the Ni and Cu malonates, with deduced effective moments of 3.41 μ_B and 1.81 μ_B, respectively. Overall, the reported values are in fair agreement with transition metals at the 2+ oxidation state in high spin configuration.

As shown on **Figure 4**, which displays the low temperature susceptibility measured in the ZFC and FC modes, all compounds, except the Cu-based one, exhibit a magnetic transition at low temperature. In the cases of Co- and Mn-malonates, the magnetic susceptibility reaches a maximum and then decreases as *T* decreases. The latter behavior, in addition to the superimposed ZFC and FC susceptibility, is typical the establishment of a AFM long-range order below T_N. On the contrary, the abrupt increase of the susceptibility at the transition in the case of Fe- and Ni-malonates, together with the divergence between ZFC and FC susceptibilities below T_N for *M*=Ni, suggests the presence of a canted AFM order. By canted AFM order, we mean here that a slight deviation from a perfectly antiparallel alignment of the spins from different sublattices results in a non-zero net magnetic moment, i.e. leads to the emergence of a weak FM component."

The above conclusions are supported by the M(H) loops of the **Figure 5**. Mn and Co-malonates exhibit closed cycles in agreement with a AFM long-range order in the absence of any magnetic field. On the other hand, Fe-and Ni-malonates show open M-H cycles, which also point towards the existence of a spontaneous net magnetization. The corresponding

remanant magnetizations are 0.26 and 0.014 μ_B/atom for Fe and Ni, respectively. A closer look at the M(H) curves reveals inflection points at $\mu_0 H \sim 1.5$ T, 6 T and 8 T in the Mn, Co and Fe-malonates, respectively, underlining weak metamagnetic components. Finally, the small values of the frustration parameters ratio ($|\theta_{CW}/T_N| < 5$) indicate the absence of frustration in these compounds.

As the Mn, Ni, Fe and Co malonates present features indicative of a long-range ordering, we used neutron powder diffraction in order to explore this possibility, and eventually solve the magnetic structures these compounds may adopt.

c) Magnetic structure determination

The magnetic structures of the malonate compounds $Na_2M(H_2C_3O_4)_2{\cdot}2H_2O$ (*M*=Mn, Fe, Co, Ni) were determined by neutron powder diffraction, on the G4.1 instrument at Laboratoire Léon Brillouin. This diffractometer presents a good resolution at low angle and a large wavelength (λ=2.423 Å) which makes it a perfect choice to explore low angle magnetic peaks. The four compounds were measured from 1.5 K to above T_N. Patterns recorded above T_N were first refined against the structural model determined from refinement of the synchrotron 11BM data taken on the same batch. An illustration of a refinement is shown in **Figure 6** for the Ni compound at 100 K, a temperature at which only the nuclear structure gives a contribution as its Néel temperature is 24(1) K.

Examination of neutron powder diffraction patterns versus T indicates that the nuclear peaks remain unchanged over the temperature range explored (only a shift of peaks with temperature is observed due to thermal expansion), indicating the absence of a structural distortion at low temperature. Moreover, when the temperature is lowered below T_N, additional peaks appear in the powder patterns (**Figure 7**). Their intensity continuously increases when the temperature is lowered to reach a maximum for T=1.5 K. Those reflections present therefore characteristics consistent with magnetic peaks arising from a long-range ordering of the magnetic moments carried by the 3*d* transition metal atoms. A first sight at the data indicates that Mn and Ni malonates present the same sequence of magnetic peaks, with the same relative intensities, therefore they will likely present a similar magnetic structure. The Co-based compound also presents the same sequence of magnetic peaks as the Ni and Mn counterparts, with in addition a tiny peak at $2\theta \approx 21°$. Lastly, the magnetic pattern

for Fe differs from the previously mentioned ones as only one magnetic reflection is clearly seen, at $2\theta \approx 21°$. For all compounds, the magnetic reflections can be indexed in the same unit cell as the nuclear structure, which gives a propagation vector **k** = (0, 0, 0). Therefore the magnetic unit cell coincides with the nuclear unit cell and contains four magnetic moments carried by the four transition metals atoms in the cell: (0, 0, ½), (½, 0, 0), (0, ½, 0) and (½, ½, ½).

A symmetry analysis was performed using Bertaut's method[37,38] in order to determine the spin configurations that are compatible with the crystal symmetry of malonate $Na_2M(H_2C_3O_4)_2 \cdot 2H_2O$. The results of this analysis (irreducible representations and their basis vectors) are detailed in Supplementary Information (**Table S1**).

As the Mn and Ni malonates present similar magnetic reflections, the magnetic structure resolution is first presented for these two compounds. We tested all the possibilities obtained by the symmetry analysis against the neutron powder patterns recorded at 1.5 K. We found that the best agreement was obtained using the Γ_1 irreducible representation (Shubnikov group *Pbca*), with magnetic moments along **c** (this corresponds to the basis function Ψ_3). Refining additional components for Ψ_1 and Ψ_2 led to values which included zero when considering the standard deviations (the maximum moments refined along the *a*-axis and *b*-axis are ~0.5 μ_B). The magnetic moments are therefore imposed to be of the form: (0, 0, ±*w*), i.e. aligned along the *c*-axis with a sign sequence (+ + − −). The Rietveld refinement of the patterns recorded at 1.5 K for Mn and Ni malonates is shown in **Figure 8.** The magnetic moments carried at 1.5 K by each of the four transition metal atoms in the cell is reported in **Table 3** while **Figure 9** shows the obtained magnetic structures, and the way two adjacent magnetic moments within a layer are coupled through the carboxylate ligand. The refined magnetic moments are 4.42(7) μ_B and 1.52(18) μ_B for *M*= Mn, and Ni respectively.

A similar approach was followed to solve the magnetic structure of $Na_2Co(H_2C_3O_4)_2 \cdot 2H_2O$. Refining moments along the *c*-axis (Γ_1 irreducible representation, Ψ_3 only), *i.e.* with a magnetic model similar to Mn and Ni, gave a decent fit with however no intensity calculated on the $2\theta=21°$ peak whose indexation is (100). The intensity of a magnetic reflection being dictated by components of magnetization perpendicular to the scattering vector, *i.e.* in our case [100]*, we refined an additional component along the b-axis (basis function Ψ_2 of Γ_1); the quality of the fit was much improved as highlighted in the inset

of **Figure 8**. The magnetic moments are of the form (0, *u*, *w*), with a spin sequence (+ − + −) and (+ + − −) for the y and z components, respectively; as a result the magnetic structure is therefore not collinear (**Table 3** and **Figure 9**). Within a layer, the Co magnetic moments (total value is 3.6(3) μ_B) are antiparallel but the direction of moments changes from one layer to another, suggesting smaller inter-plane antiferromagnetic interactions than for the Mn and Ni compounds.

Lastly, we examine the case of the Fe-based malonate, which presents at 2θ=21° its most intense magnetic reflection. Unfortunately we noticed that the sample contained a small amount of impurities because it slightly evolved with time between the synchrotron and neutron experiments. However, this did not prevent us from solving the structure, as these impurity peaks do not overlap with the magnetic reflections. The magnetic structure determination was performed on the difference pattern (1.5 K – 17 K). 17 K was chosen because it is the lowest temperature above the Néel temperature (T_N=16 K). The magnetic contribution to the pattern could be approximately fitted with the Γ_7 irreducible representation (Shubnikov group *Pbc'a'*) with moments along *z* (basis function $\mathbf{\Psi}_3$), however the best fit was obtained with Γ_1 (Shubnikov group *Pbca*, same as the other counterparts) with components along *y* only ($\mathbf{\Psi}_2$). **Figure 10** illustrates the simulated patterns from the two magnetic structures mentioned above together with the experimental difference pattern. The refinement was then carried out on the pattern recorded at 1.5 K (**Figure 8**), and fully confirms the *Pbca* magnetic structure (Γ_1 representation). A magnetic moment of 3.42(29) μ_B is obtained (**Table 3).** Fe moments in $Na_2Fe(H_2C_3O_4)_2{\cdot}2H_2O$ follow the sign sequence (+ − + −) and are oriented along the *b*-axis: they are of the form (0, ±*v*, 0).

Our neutron diffraction study indicates that all compounds display a magnetic structure in the *Pbca* Shuknikov group characterized by antiferromagnetic layers. However, the crystallographic orientation of the moment and the stacking of these AF layers depend on the nature of the transition metal. Mn^{2+} and Ni^{2+} have their moments along [001] and the layers are stacked parallel in the (a, c) plane. Co^{2+} presents an additional component along [010], which becomes prominent for the Fe^{2+} analog. For the latter, moments are along [010] and Fe-malonate layers are antiparallely stacked in the (a,c) plane. The magnetic moments at 1.5 K for Mn, Fe and Ni are 4.42(7) μ_B, 3.42(29) μ_B and 1.52(18) μ_B, respectively; these values are systematically below the spin-only expected value (g·S = 5 μB, 4 μB and 2 μB for the d^5, d^6 and d^8 ions, respectively), as seen in **Table 2**. The magnetic moment reduction has

been often observed in other compounds and may be due to covalency by electron transfer toward the anions and/or zero-point fluctuations of the antiferromagnetic ground state. Conversely, the experimental magnetic moment (3.6(3) μ_B) for Co^{2+} (d^7) is slightly larger than the theoretical value of 3 μB, which indicates a small contribution of the orbital moment, as often observed for cobalt.[39–41]

Notice that we could not find evidence from neutron scattering of the tiny canting seen by magnetization measurements for the Fe and Ni-based compounds, which is also not permitted in the Γ_1 representation. The possibility of a mixture of representations cannot be excluded, and single crystal neutron diffraction would be necessary to investigate the presence of possible weak ferromagnetic components.

d) Theoretical estimation of the magnetic couplings

To get insights into the mechanisms that favor the establishment of the long-range magnetic order for the Mn, Fe, Co and Ni malonates, we have calculated the isotropic magnetic couplings up to the fifth nearest-neighbors in GGA+U_{scf} using the procedure described in the *Experimental and computational details* section. The results are summarized in **Table 4**. These couplings are represented in **Figure 9** (right panel) and numbered according to increasing metal-metal distance: J_1 corresponds to the nearest neighbor coupling within the (*a*,*b*) planes whereas J_2 and J_4 correspond to the second and third nearest-neighbors within the planes (respectively, along the *a* and *b* crystallographic directions). J_3 and J_5 are the interplane couplings located either in the (*a*,*c*) plane or in the (*b*,*c*) plane.

The calculated amplitudes have to be considered on a semi-quantitative basis only both because of their well-known dependence with respect to the actual exchange-correlation functional employed in the calculations (see for example, ref 42), but also because of the geometry of these coordination compounds involving weak and very long-ranged magnetic couplings. DFT results, however, deliver a clear picture of the magnetism of this series of compounds where the nearest-neighbor coupling J_1 within the (*a*,*b*) planes is largely dominant. This is consistent with the fact that J_1 is the only magnetic coupling corresponding to a well-defined covalent O-C-O carboxylate bridge. Moreover, J_1 is antiferromagnetic for the Mn, Co and Ni-malonates whereas it becomes ferromagnetic in the case of Cu, in remarkable agreement with the results deduced from the magnetic susceptibilities. Note that our findings are fully consistent with the ferromagnetic coupling observed in other copper-

carboxylate based compounds, and with antiferromagnetic interactions for Co^{2+}, Ni^{2+}, Mn^{2+} and Fe^{2+} carboxylates.[8,12–14]

Additional second and third nearest neighbor interactions within the (*a*,*b*) plane (J_2 and J_4) are much weaker and as such, confirm the absence of sizeable frustration in these planes. Calculated interplane interactions are also vanishingly weak as it could be anticipated from the corresponding large spatial separation between transition metal ions (~9 Å) and the absence of clear superexchange path through Na^+ ions and H_2O molecules in the interplane region. However, we should stress here that zero values appearing in **Table 4** do not indicate that these couplings are strictly absent in the Mn and Co compounds but that they are too weak to be evaluated by our method. Their amplitude should therefore be one or two orders of magnitude weaker than the nearest-neighbor interaction J_1. The only sizeable J_3 and J_5 couplings calculated with this method are obtained in the case of the Ni-malonate: both are antiferromagnetic and of the same order of magnitude. Whereas a three-dimensional ordering can therefore be expected, as observed experimentally by neutron diffraction, the exact stacking of antiferromagnetic (*a*,*b*) planes along the *c* direction cannot be assessed.

e) Discussion

Although neutron diffraction experiments assess the presence of non-negligible interplane couplings, leading eventually to the experimental observation of a three-dimensional long-range magnetic order at low temperature, density functional calculations emphasize the much larger amplitude of the intraplane nearest-neighbor coupling J_1 as compared to the interlayer ones in this series of compounds. The picture delivered by these calculations is therefore that of weakly coupled 2D antiferromagnetic layers (except in the case of Cu). Assuming therefore that these layers can be considered, in first approximation, as isolated and topologically equivalent to an antiferromagnetic square lattice, the high-temperature magnetic susceptibility can be modeled using the parameterization given by Lines[43]:

$$\chi = \frac{N g^2 \mu_B^2}{J_1} \frac{1}{3\theta + \sum_n \frac{C_n}{\theta^{n-1}}} + \chi_0$$

Eq. 6

where $\theta = -k_B T/J_1 S(S+1)$, μ_B is the Bohr magneton, and N is the number of spins in the lattice. This parameterization is based on an isotropic Heisenberg Hamiltonian and as such, can only be applied to systems with vanishing orbital contribution to the magnetic moment. As this is only true for the Mn-malonate, we will essentially focus our discussion on this member of the series. For S=5/2, the coefficients C_n are given by C_1=4, C_2=1.448, C_3=0.228, C_4=0.262, C_5=0.119 and C_6=0.017.

The result of the fit obtained for $T > T_N$ is shown in **Figure 11**. An excellent agreement is found for a value of the nearest neighbor interaction J_1 = 1.3K, very close to the value predicted in DFT. Furthermore, the mean-field expression of the Curie-Weiss temperature in terms of various magnetic couplings arising in a compound is given by [44]:

$$\theta_{CW} = -\frac{S(S+1)}{3k_B}\sum_{m=1}^{N'} z_m J_m$$

Eq. 7

where z_m is the number of m^{th} nearest neighbors of a given atom and J_m is the exchange interaction between m^{th} neighbors. Limiting the calculation to the nearest-neighbors (z_1=4), as suggested by the excellent agreement obtained for the fit of the magnetic susceptibility and the results obtained in DFT, Eq. 7 gives a value of θ_{CW} = -15.1 K, in very good agreement with the experimental value of -17.3 K (see Table 2). Mn-malonate therefore appears as a very close realization of weakly coupled 2D antiferromagnetic square lattice. This analysis cannot be easily extended to the other members of the series (Fe, Co, Ni) where a substantial orbital contribution to the magnetic moment is observed. Structural similarities, however, strongly suggest that this dominating in-plane 2D antiferromagnetism is also present in these compounds. For instance, a very similar phenomenology is observed in Co-malonate and is confirmed by DFT calculations. Lines model for the square lattice[43] predicts a temperature $T_{\chi max.}$ at which the susceptibility reaches its maximum located at:

$$\frac{k_B T_{\chi max.}}{J_1} = 1.12S(S+1) + 0.1$$

Eq.8

which gives, using the estimated value J_1 = 5.1 K from DFT calculations, $T_{\chi max.}$ = 22 K in qualitative agreement with the experiments as seen in **Figure 4**.

Conclusion

Using magnetization measurements and neutron powder diffraction, we have explored and solved the magnetic structures of a series of metal malonate compounds of formulae $Na_2M(H_2C_3O_4)_2{\cdot}2H_2O$ where *M* is a 3*d* transition metal at the 2+ oxidation state. The magnetic behavior of this series of compounds at high and intermediate temperatures is dominated by 2D antiferromagnetism essentially through a dominant nearest-neighbor interaction supported by O-C-O carboxylate bridges between the M^{2+} atoms at a distance varying between 5.70 and 5.85 Å. Other more distant interactions are much weaker but not negligible as they eventually lead to a 3D antiferromagnetic ordering a low temperature. Magnetic moments within layers are coupled antiferromagnetically through carboxylate groups, and neutron diffraction reveals that the direction of moments is [001] for the *M*=Mn, Ni malonates and along [010] for *M*=Fe. In the (a,c) plane, the resulting antiferromagnetic layers are stacked parallel for the former and antiparallel for the latter. The Co-malonate presents an intermediate situation between the two latter, resulting in a non-collinear magnetic structure. Overall, these malonate magnetic structures all belong to the *Pbca* Shubnikov group. This family of compounds displays a phenomenology shared by many TM molecular based materials. In particular, the presence of a dominating in-plane 2D antiferromagnetism for the divalent Mn, Fe, Co and Ni members is indeed frequently met in layered compounds. One of the main findings of this work therefore consists in the demonstration that, although lower-dimensionality models can accurately describe the magnetism of these compounds at high and intermediate temperatures, their low temperature behavior is systematically characterized by the occurrence of a 3D long range ordering. This general picture is certainly shared by many other metal-carboxylates and as such, strengthens the relevance of neutron diffraction to unravel their magnetic properties.

Acknowledgments

Authors thank Nadir Recham and Jean-Marie Tarascon for fruitful discussions, Françoise Damay and Gilles André for their help in neutron scattering experiments, Benoît Baptiste for

help in diffraction experiments and LLB for allocated beamtime. Use of the 11-BM mail service of the APS at Argonne National Laboratory was supported by the U.S. Department of Energy under Contract No. DE-AC02-06CH11357 and is greatly acknowledged. This work was granted access to the High Performance Computing resources of Institut du Développement et des Ressources en Informatique Scientique under the allocations 2014-100384 and 2015-100384 made by Grand Equipement National de Calcul Intensif.

References

1 G. Givaja, P. Amo-Ochoa, C. J. Gómez-García and F. Zamora, *Chem. Soc. Rev.*, 2012, **41**, 115–147.
2 S. Kitagawa, R. Kitaura and S. Noro, *Angewandte Chemie International Edition*, 2004, **43**, 2334–2375.
3 G. Férey, *Chem. Soc. Rev.*, 2008, **37**, 191–214.
4 O. M. Yaghi, M. O'Keeffe, N. W. Ockwig, H. K. Chae, M. Eddaoudi and J. Kim, *Nature*, 2003, **423**, 705–714.
5 C. Ruiz-Pérez, Y. Rodríguez-Martín, M. Hernández-Molina, F. S. Delgado, J. Pasán, J. Sanchiz, F. Lloret and M. Julve, *Polyhedron*, 2003, **22**, 2111–2123.
6 Z. Wang, K. Hu, S. Gao and H. Kobayashi, *Advanced Materials*, 2010, **22**, 1526–1533.
7 M. Liang, Q.-L. Wang, L.-H. Yu, D.-Z. Liao, Z.-H. Jiang, S.-P. Yan and P. Cheng, *Polyhedron*, 2004, **23**, 2203–2208.
8 J. Pasán, F. S. Delgado, Y. Rodríguez-Martín, M. Hernández-Molina, C. Ruiz-Pérez, J. Sanchiz, F. Lloret and M. Julve, *Polyhedron*, 2003, **22**, 2143–2153.
9 F. S. Delgado, C. A. Jiménez, P. Lorenzo-Luis, J. Pasán, O. Fabelo, L. Cañadillas-Delgado, F. Lloret, M. Julve and C. Ruiz-Pérez, *Crystal Growth & Design*, 2012, **12**, 599–614.
10 L. Cañadillas-Delgado, O. Fabelo, J. A. Rodríguez-Velamazán, M.-H. Lemée-Cailleau, S. A. Mason, E. Pardo, F. Lloret, J.-P. Zhao, X.-H. Bu, V. Simonet, C. V. Colin and J. Rodríguez-Carvajal, *Journal of the American Chemical Society*, 2012, **134**, 19772–19781.
11 O. Fabelo, L. Cañadillas-Delgado, J. Pasán, F. S. Delgado, F. Lloret, J. Cano, M. Julve and C. Ruiz-Pérez, *Inorganic Chemistry*, 2009, **48**, 11342–11351.
12 F. Su, L. Lu, S. Feng, M. Zhu, Z. Gao and Y. Dong, *Dalton Trans.*, 2015, **44**, 7213–7222.
13 E. Colacio, J. M. Dominguez-Vera, M. Ghazi, R. Kivekäs, M. Klinga and J. M. Moreno, *European journal of inorganic chemistry*, 1999, 441–446.
14 F. S. Delgado, J. Sanchiz, C. Ruiz-Pérez, F. Lloret and M. Julve, *Inorganic Chemistry*, 2003, **42**, 5938–5948.
15 I. G. de Muro, M. Insausti, L. Lezama, M. K. Urtiaga, M. I. Arriortua and T. Rojo, *Journal of the Chemical Society, Dalton Transactions*, 2000, 3360–3364.
16 I. Gil de Muro, L. Lezama, M. Insausti and T. Rojo, *European Journal of Inorganic Chemistry*, 2003, **2003**, 2948–2954.
17 Y. Rodríguez-Martín, M. Hernández-Molina, J. Sanchiz, C. Ruiz-Pérez, F. Lloret and M. Julve, *Dalton Transactions*, 2003, 2359–2365.
18 T. K. Maji, S. Sain, G. Mostafa, T.-H. Lu, J. Ribas, M. Monfort and N. R. Chaudhuri, *Inorganic Chemistry*, 2003, **42**, 709–716.
19 I. G. de Muro, F. A. Mautner, M. Insausti, L. Lezama, M. I. Arriortua and T. Rojo, *Inorganic Chemistry*, 1998, **37**, 3243–3251.
20 P. Diaz-Gallifa, O. Fabelo, J. Pasan, L. Canadillas-Delgado, J. Rodriguez-Carvajal, F. Lloret, M. Julve and C. Ruiz-Perez, *Inorg. Chem.*, 2014, **53**, 5674–5683.

21 O. Fabelo, L. Canadillas-Delgado, J. Pasan, P. Diaz-Gallifa, C. Ruiz-Perez, F. Lloret, M. Julve, I. P. Orench, J. Campo and J. Rodriguez-Carvajal, *Inorg. Chem.*, 2013, **52**, 12818–12827.
22 A. Mesbah, R. Sibille, T. Mazet, B. Malaman, S. Lebegue and M. Francois, *J. Mater. Chem.*, 2010, **20**, 9386–9391.
23 D. Ghoshal, T. Kumar Maji, T. Mallah, T.-H. Lu, G. Mostafa and N. R. Chaudhuri, *Inorganica Chimica Acta*, 2005, **358**, 1027–1033.
24 H. Ahouari, G. Rousse, Y. Klein, J.-N. Chotard, M. T. Sougrati, N. Recham and J.-M. Tarascon, *Solid State Sciences*, 2015, **42**, 6–13.
25 H. M. Rietveld, *Journal of Applied Crystallography*, 1969, **2**, 65–71.
26 J. Rodríguez-Carvajal, *FullProf Suite*, .
27 P. Giannozzi, S. Baroni, N. Bonini, M. Calandra, R. Car, C. Cavazzoni, D. Ceresoli, G. L. Chiarotti, M. Cococcioni, I. Dabo, A. Dal Corso, S. de Gironcoli, S. Fabris, G. Fratesi, R. Gebauer, U. Gerstmann, C. Gougoussis, A. Kokalj, M. Lazzeri, L. Martin-Samos, N. Marzari, F. Mauri, R. Mazzarello, S. Paolini, A. Pasquarello, L. Paulatto, C. Sbraccia, S. Scandolo, G. Sclauzero, A. P. Seitsonen, A. Smogunov, P. Umari and R. M. Wentzcovitch, *Journal of Physics: Condensed Matter*, 2009, **21**, 395502.
28 K. F. Garrity, J. W. Bennett, K. M. Rabe and D. Vanderbilt, *Computational Materials Science*, 2014, **81**, 446–452.
29 J. P. Perdew, K. Burke and M. Ernzerhof, *Physical Review Letters*, 1996, **77**, 3865–3868.
30 M. Cococcioni and S. de Gironcoli, *Physical Review B*, 2005, **71**, 035105.
31 H. J. Kulik, M. Cococcioni, D. A. Scherlis and N. Marzari, *Physical Review Letters*, 2006, **97**, 103001.
32 G. Radtke, A. Saúl, H. A. Dabkowska, G. M. Luke and G. A. Botton, *Physical Review Letters*, 2010, **105**, 036401.
33 A. Saúl and G. Radtke, *Physical Review Letters*, 2011, **106**, 177203.
34 A. Saúl, D. Vodenicarevic and G. Radtke, *Physical Review B*, 2013, **87**, 024403.
35 A. Saúl and G. Radtke, *Physical Review B*, 2014, **89**, 104414.
36 F. E. Mabbs and D. J. Machin, *Magnetism and Transition Metal Complexes*, Dover Publications, Mineola, N.Y, 2008.
37 E. F. Bertaut, *Acta Crystallographica Section A: Crystal Physics, Diffraction, Theoretical and General Crystallography*, 1968, **24**, 217–231.
38 E. F. Bertaut, *J. Phys. Colloques*, 1971, **32**, C1–462–C1–470.
39 B. C. Melot, G. Rousse, J.-N. Chotard, M. C. Kemei, J. Rodríguez-Carvajal and J.-M. Tarascon, *Physical Review B*, 2012, **85**.
40 B. C. Melot, J. N. Chotard, G. Rousse, M. Ati, M. Reynaud and J. M. Tarascon, *Inorganic Chemistry*, 2011, **50**, 7662–7668.
41 M. Reynaud, G. Rousse, J.-N. Chotard, J. Rodríguez-Carvajal and J.-M. Tarascon, *Inorganic Chemistry*, 2013, **52**, 10456–10466.
42 R. L. Martin and F. Illas, *Physical review letters*, 1997, **79**, 1539.
43 M. E. Lines, *J. Phys. Chem. Solids*, 1970, **31**, 101–116.
44 J. S. Smart, *Effective field theories of magnetism*, Saunders, Philadelphia; London, 1966.
45 H. Fuess, T. Hahn, H. Wondratschek, U. Müller, U. Shmueli, E. Prince, A. Authier, V. Kopsky, D. B. Litvin, G. Rossman, E. Arnold, S. Hall and B. McMahon, Eds., *International Tables for Crystallography*, Springer., 2007, vol. A-G.

List of Tables

Table 1. Structural parameters for malonate $Na_2Mn(H_2C_3O_4)_2{\cdot}2H_2O$ deduced from the Rietveld refinement of Synchrotron X-ray diffraction. Lattice parameters and unit cell volumes for *M*=Ni, Co, Fe and Cu are also indicated.

Atom	Wyckoff site	*X*	*y*	*z*	B(Å^2)
Mn	4*b*	0	0	0.5	1.182(13)
O1	8*c*	0.1194(3)	0.5738(2)	-0.11039(12)	1.13(4)
O2	8*c*	0.0626(3)	0.7018(2)	0.05468(12)	1.40(5)
O3	8*c*	0.2923(3)	0.49599(17)	0.20290(10)	1.77(4)
O4	8*c*	0.2028(3)	0.7616(2)	0.30053(12)	1.56(5)
O5	8*c*	-0.2840(3)	0.5917(2)	-0.04445(12)	1.47(5)
C1	8*c*	0.1376(5)	0.7987(4)	0.36771(18)	1.32(7)
C2	8*c*	0.0709(3)	0.8192(3)	-0.0754(2)	1.05(7)
H1	8*c*	0.384(3)	0.445(2)	0.1712(12)	2*
H2	8*c*	0.264(4)	0.4243(18)	0.2413(11)	2*
C3	8*c*	0.1213(5)	0.8069(3)	0.0126(2)	1.59(7)
Na	8*c*	-0.0017(2)	0.62352(12)	0.20419(7)	1.97(3)
H3	8*c*	0.131(3)	0.8973(16)	-0.0978(14)	2*
H4	8*c*	-0.4361(8)	0.311(3)	-0.0855(15)	2*

*= not refined

Reliability parameters: χ^2=1.13; Synchrotron: Bragg R-factor=6.59%

Space Group: *Pbca*
***M*=Mn** *a*=6.831841(4) Å, *b*=9.518045(6) Å, *c*=16.519062(10) Å, *V*= 1074.165(2) Å^3
***M*=Ni** *a*=6.785604(7) Å, *b*=9.215804(10) Å, *c*=16.559155(17) Å *V*=1035.523(2) Å^3
***M*=Co** *a*=6.788764(6) Å, *b*=9.332060(8) Å, *c*=16.523726(14) Å *V*=1046.830(2) Å^3
***M*=Fe** *a*=6.79211(2) Å, *b*=9.45249(4) Å, *c*=16.48661(7) Å *V*=1058.480(3) Å^3
***M*=Cu** *a*= 6.83606(7) Å, *b*= 9.50212(12) Å, *c*=16.39482(19) Å *V*= 1064.96(3) Å^3

Table 2. Magnetic parameters of malonate compounds deduced from magnetic measurements and compared to expected theoretical values. *T_N is given by the maximum of d(χT)/dT

	Mn^{2+}	Fe^{2+}	Co^{2+}	Ni^{2+}	Cu^{2+}
Electronic configuration	$d^5:t_{2g}^3e_g^2$	$d^6:t_{2g}^4e_g^2$	$d^7:t_{2g}^5e_g^2$	$d^8:t_{2g}^6e_g^2$	$d^9:t_{2g}^6e_g^3$
in octahedral field	*S=5/2, L=0*	*S=2, L=2*	*S=3/2, L=3*	*S=1, L=3*	*S=1/2, L=2*
Expected Theoretical Values					
Effective moment, μ_{eff}					
$\mu_{eff}=g_j[J(J+1)]^{1/2}$	5.92 μ_B	6.71 μ_B	6.63 μ_B	5.59 μ_B	3.38 μ_B
$\mu_{eff}=[4S(S+1)+L(L+1)]^{1/2}$	5.92 μ_B	5.48 μ_B	5.20 μ_B	4.47 μ_B	3 μ_B
$\mu_{eff}=2.[S(S+1)]^{1/2}$	5.92 μ_B	4.90 μ_B	3.87 μ_B	2.83 μ_B	1.73 μ_B
Saturation (spin only), m=g.S	5 μ_B	4 μ_B	3 μ_B	2 μ_B	1 μ_B
Experimental Values Deduced from Magnetic Measurements					
$Na_2M(H_2C_3O_4)_2\cdot 2H_2O$					
Néel temperature, T_N (K)	8(1)	16(1)	13(1)	24(1)	-
Curie constant, C_m (emu K mol^{-1})	4.45	3.51	3.35	1.41	0.41
Curie-Weiss temperature θ_{CW} (K)	-17.3(1)	-23.0(1)	-58.0(3)	-60(1)	1.6(1)
Effective moment, μ_{eff} (μ_B)	5.95	5.29	5.22	3.41	1.81
$\lvert\theta_{CW}/T_N\rvert$	2.16(6)	1.35(5)	4.46(2)	2.50(2)	-

Table 3: Magnetic moments (in terms of components along the *a, b* and *c* axis) for the four transition metals of the unit cell. Values and directions of moments are obtained from the refinement of the neutron powder pattern at 1.5 K.

	Magnetic moments in $Na_2M(H_2C_3O_4).2H_2O$			
Position of *M* in unit cell	*M*=Mn	*M*=Co	*M*=Ni	*M*=Fe
M(0, 0, ½)	(0, 0, +4.42(7) μ_B)	(0, +2.34(22) μ_B, –2.79(10) μ_B)	(0, 0, +1.52(18) μ_B)	(0, +3.43(29) μ_B, 0)
M(½, 0, 0)	(0, 0, +4.42(7) μ_B)	(0, –2.34(22) μ_B, –2.79(10) μ_B)	(0, 0, +1.52(18) μ_B)	(0, –3.43(29) μ_B, 0)
M(0, ½, 0)	(0, 0, –4.42(7) μ_B)	(0, +2.34(22) μ_B, +2.79(10) μ_B)	(0, 0, –1.52(18) μ_B)	(0, +3.43(29) μ_B, 0)
M(½, ½, ½)	(0, 0, –4.42(7) μ_B)	(0, –2.34(22) μ_B, +2.79(10) μ_B)	(0, 0, –1.52(18) μ_B)	(0, –3.43(29) μ_B, 0)
Total magnetic moment	4.42(7) μ_B	3.6(3) μ_B	1.52(18) μ_B	3.43(29) μ_B

Table 4: Magnetic couplings up to the fifth nearest neighbors obtained in GGA+U_{scf} for Mn, Co, Ni and Cu-malonates. Numerical values are given in Kelvin. According to the convention used in Equation 1, positive couplings are antiferromagnetic.

Couplings (K)	Mn (S=5/2)	Co (S=3/2)	Ni (S=1)	Cu (S=1/2)
J_1	1.0	5.1	34.5	-2.4
J_2	~ 0.0	~ 0.0	2.2	~ 0.0
J_3	~ 0.0	~ 0.0	6.7	0.2
J_4	~ 0.0	~ 0.0	2.1	0.1
J_5	~ 0.0	~ 0.0	6.9	0.2

Figure Captions

Figure 1 : Rietveld refinement of Synchrotron (a,b,c) and laboratory (d,e) diffraction patterns of malonate $Na_2M(H_2C_3O_4)\cdot 2H_2O$ compounds, with *M*=Mn, Co, Ni, Fe, Cu respectively. The red crosses, black continuous line and bottom dark gray line represent the observed, calculated, and difference patterns, respectively. Vertical blue tick bars are the Bragg positions. For M=Mn, Co, Fe and Cu, tiny amounts of NaCl are found in the powder (2^{nd} line of vertical tick bars).

Figure 2: Structure of $Na_2M(H_2C_3O_4)_2\cdot 2H_2O$ (here for *M*=Mn). a) and b) general view of the unit cell content along [010] and [100], respectively. c) single layer of MO_6 octahedra and malonate groups. d) zoom on the connectivity between M and malonate groups, highlighting the *anti-anti* bridging mode of the carboxylate. Na is yellow, *M* is purple, O is red, C is brown, H is light gray.

Figure 3: Temperature dependence of the inverse magnetic susceptibility ($1/\chi$) of $Na_2M(H_2C_3O_4)_2\cdot 2H_2O$ (*M*=Mn, Fe, Co, Ni, and Cu) measured under zero field cooling (ZFC) conditions with a field of 10 kOe. The diamagnetic component from the sample holder and core diamagnetism were subtracted. The red lines represent the best fits to the Curie-Weiss law.

Figure 4: Low temperature dependence of the magnetic susceptibility (χ) of $Na_2M(H_2C_3O_4)_2\cdot 2H_2O$ (*M*=Mn, Fe, Co, and Ni) measured under zero field cooling (ZFC) and field cooling (FC) conditions.

Figure 5: M versus H hysteresis loops of $Na_2M(H_2C_3O_4)_2\cdot 2H_2O$ (*M*=Mn, Fe, Co, and Ni) measured at a temperature of 5 K.

Figure 6: Rietveld refinement of neutron powder pattern of malonate $Na_2Ni(H_2C_3O_4)\cdot 2H_2O$ at 100 K, i.e. well above the Néel temperature (24 K). The red crosses, black continuous line and bottom gray line represent the observed, calculated, and difference patterns, respectively. Vertical blue tick bars are the Bragg positions. Tiny amounts of NaCl were included as second phase in the refinement (2^{nd} line of vertical tick bars).

Figure 7: Evolution of the neutron powder patterns of malonate $Na_2M(H_2C_3O_4)_2\cdot 2H_2O$ (*M*=Mn, Co, Ni, Fe) with temperature. Below T_N (patterns colored in blue), note the appearance of new peaks of magnetic origin in addition to the nuclear peaks observed above T_N (patterns colored in red). The black arrow highlights the position of these magnetic reflections.

Figure 8: Rietveld refinement of neutron powder patterns of malonate $Na_2M(H_2C_3O_4)\cdot 2H_2O$ at 1.5 K, for *M*=Mn, Co, Ni and Fe. The red crosses, black continuous line and bottom gray line represent the observed, calculated, and difference patterns, respectively. Vertical blue tick bars are the Bragg positions: 1^{st} line: nuclear; 2^{nd} line: magnetic reflections. Tiny amounts of NaCl were included as second phase in the refinement (3rd line of vertical tick bars). The inset for *M*=Co is a zoom on the (100) magnetic reflection (marked with an arrow). For *M*=Fe, the star symbol indicates the presence of a minority phase arising from time aging; these peaks do not evolve with T and are not representative of the sample. (Reliability factors: *M*=Mn: R_{Bragg}=5.07%, magnetic R_{Bragg}=8.17%; *M*=Co: R_{Bragg}=6.16%, magnetic

R_{Bragg}=13.4%; *M*=Ni: R_{Bragg}=1.93%, magnetic R_{Bragg}=15%; M=Fe: R_{Bragg}=6.82%, magnetic R_{Bragg}=8.15%).

Figure 9: Illustration of the magnetic structures deduced from neutron powder diffraction. Red arrows represent the magnetic moments carried by the transition metal atoms (purple balls). For sake of clarity, non-magnetic atoms are not represented in the upper part but an enlarged view of the carboxylate-bridging is plot in the lower part of the figure. The right part presents the two magnetic interactions to be considered in $Na_2M(H_2C_3O_4)\cdot 2H_2O$: J_1, J_2 and J_4 are intralayer interactions, while J_3 and J_5 are interlayer interactions.

Figure 10: Comparison between the neutron difference pattern (1.5 K - 17 K) of $Na_2Fe(H_2C_3O_4)\cdot 2H_2O$ (bottom black line), and the magnetic simulated pattern for the two best models: Shubnikov group *Pbca*, Γ_1 with moments along **b** (middle blue pattern) and Shubnikov group *Pbc'a'*, Γ_7 with moments along **c** (top orange pattern). The former is clearly in better agreement with experimental data than the latter.

Figure 11: Fit of the magnetic susceptibility for the Mn-malonate in the 8-350 K range using Equation 6 with S=5/2. The open points correspond to the experiments, and the solid line corresponds to the best fit, obtained with J_1 = 1.3 K.

Figure 1

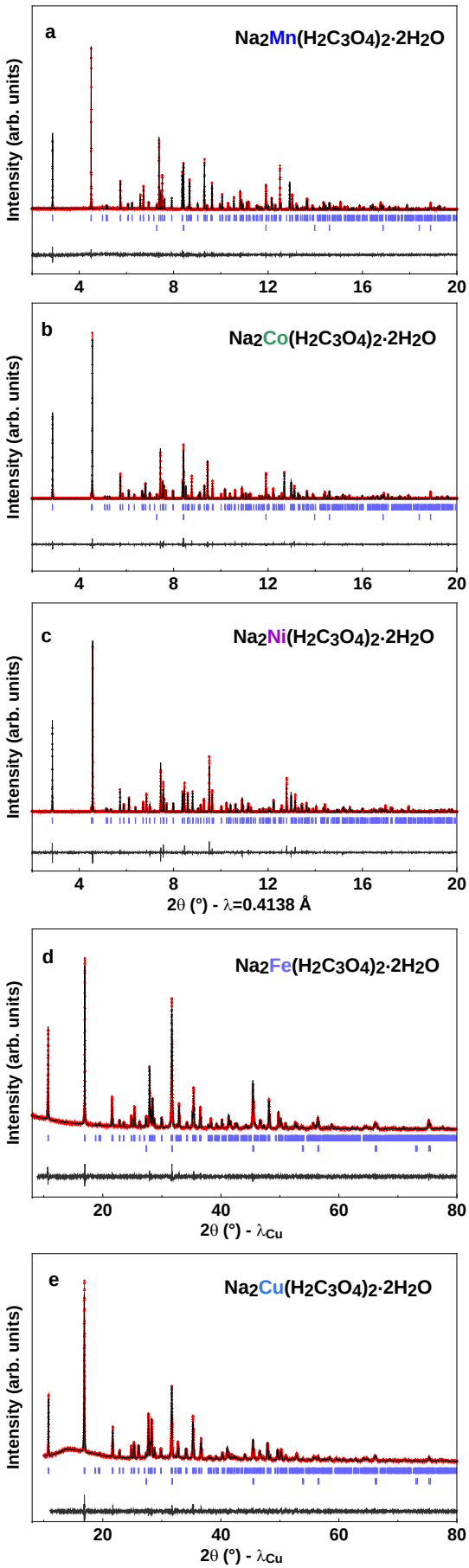
a
Na2Mn(H2C3O4)2·2H2O
b
Na2Co(H2C3O4)2·2H2O
c
Na2Ni(H2C3O4)2·2H2O
d
Na2Fe(H2C3O4)2·2H2O
e
Na2Cu(H2C3O4)2·2H2O
Intensity (arb. units)
2θ (°) - λ=0.4138 Å
2θ (°) - λCu

Figure 2

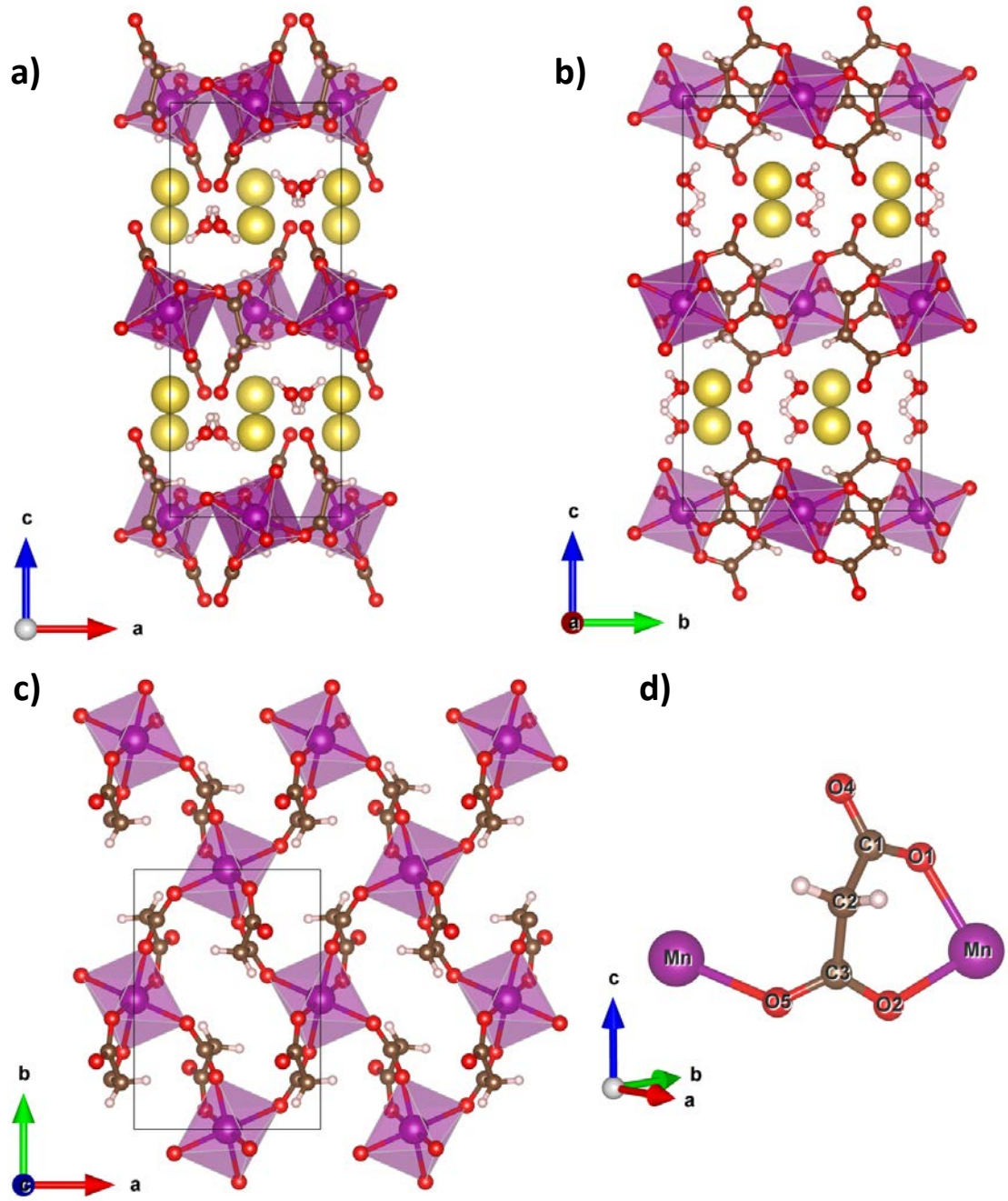

Figure 3

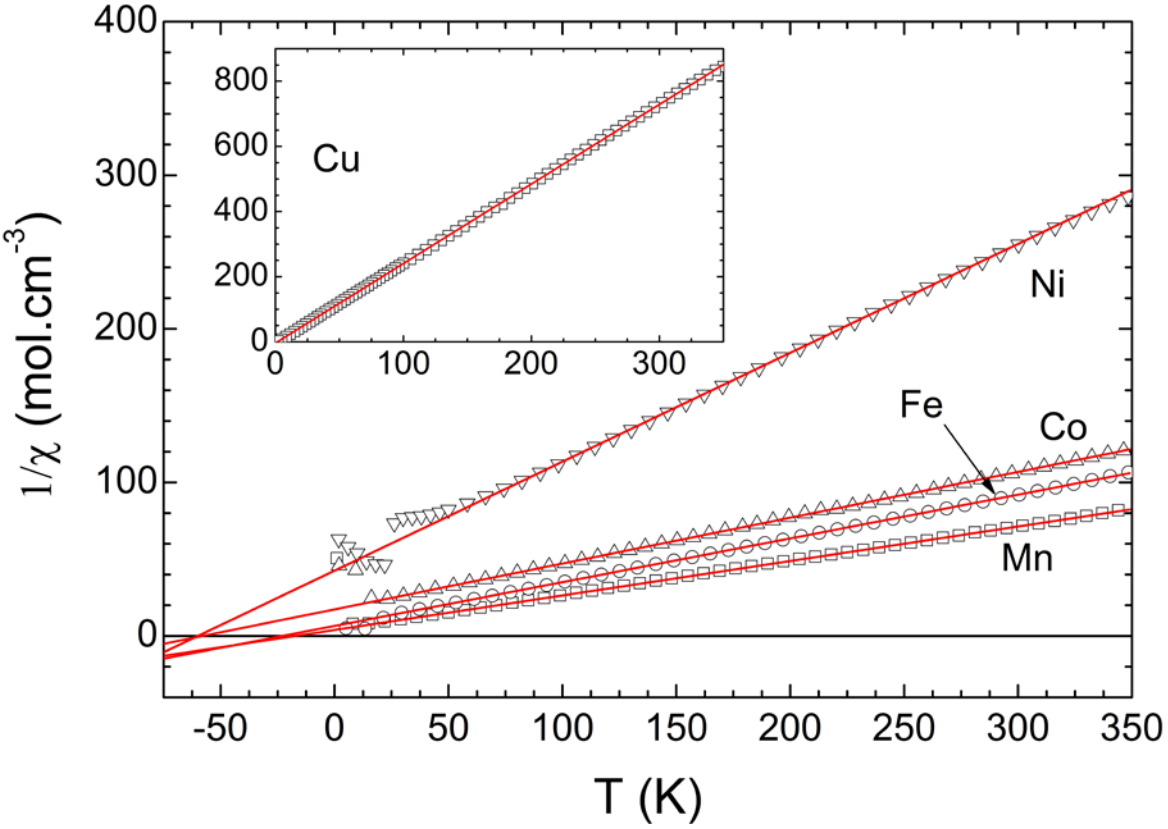
400
300
200
100
0
-50
0
50
100
150
200
250
300
350
T (K)
1/χ (mol.cm-3)
Ni
Fe
Co
Mn
800
600
400
200
0
0
100
200
300
Cu

Figure 4

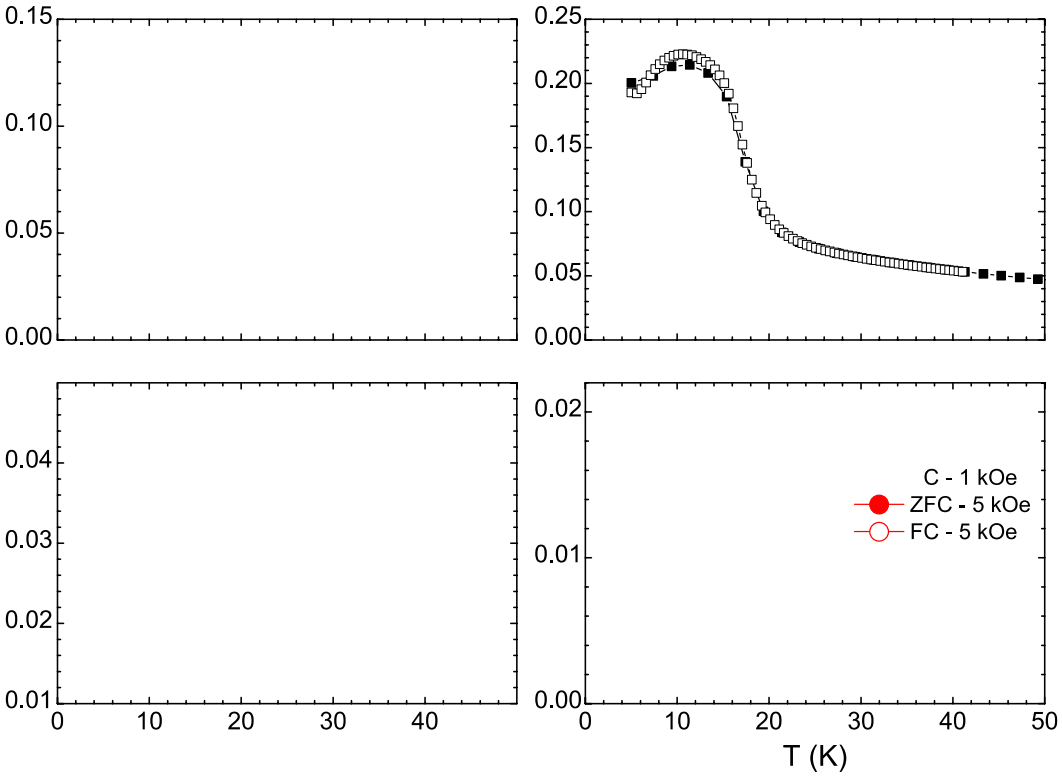
0.15
0.10
0.05
0.00
0.25
0.20
0.15
0.10
0.05
0.00
0.04
0.03
0.02
0.01
0.02
0.01
0.00
0
10
20
30
40
0
10
20
30
40
50
T (K)
C - 1 kOe
ZFC - 5 kOe
FC - 5 kOe

Figure 5

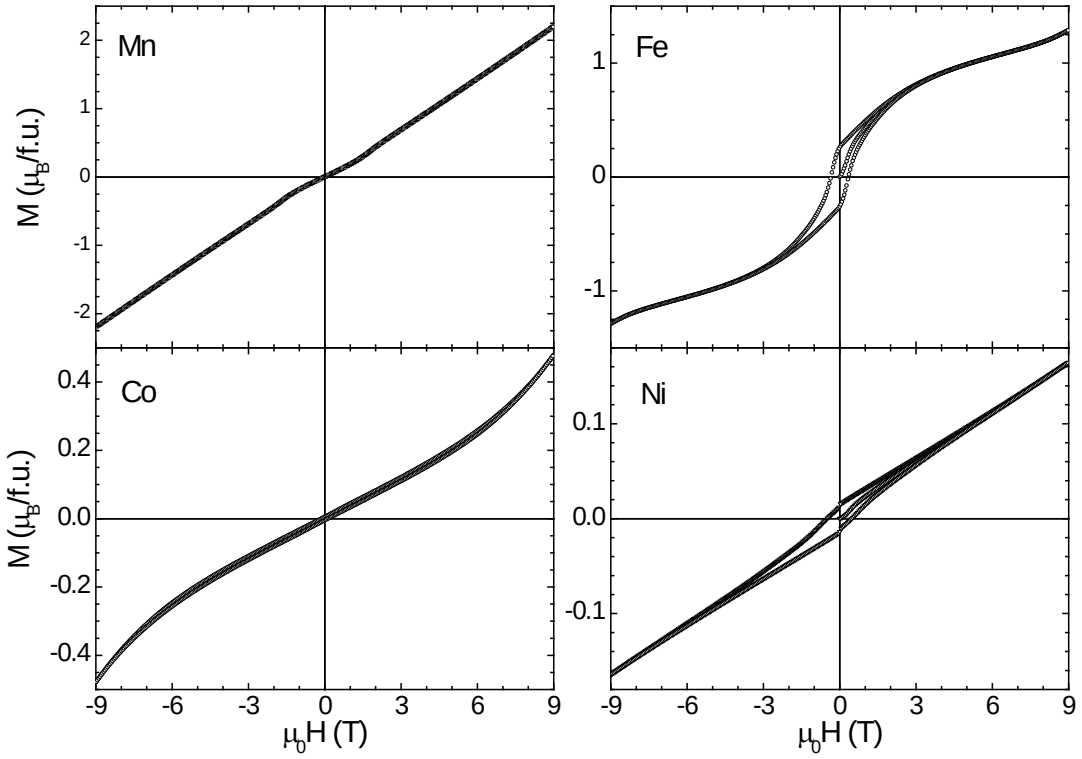

Figure 6

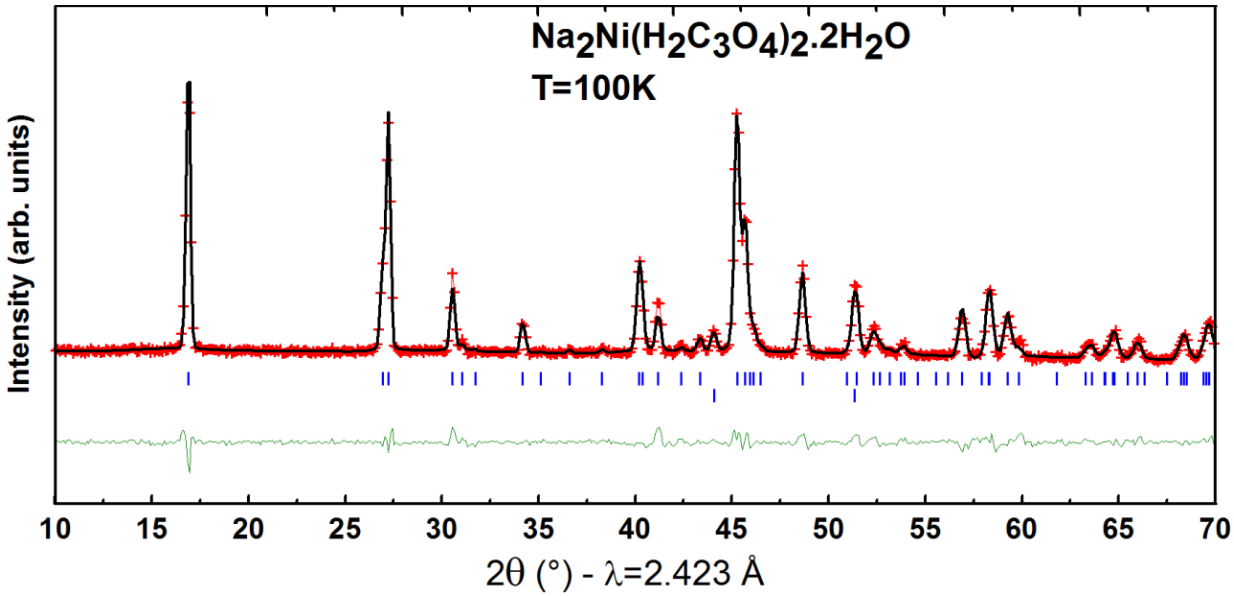
Na2Ni(H2C3O4)2.2H2O
T=100K
Intensity (arb. units)
10
15
20
25
30
35
40
45
50
55
60
65
70
2θ (°) - λ=2.423 Å

Figure 7

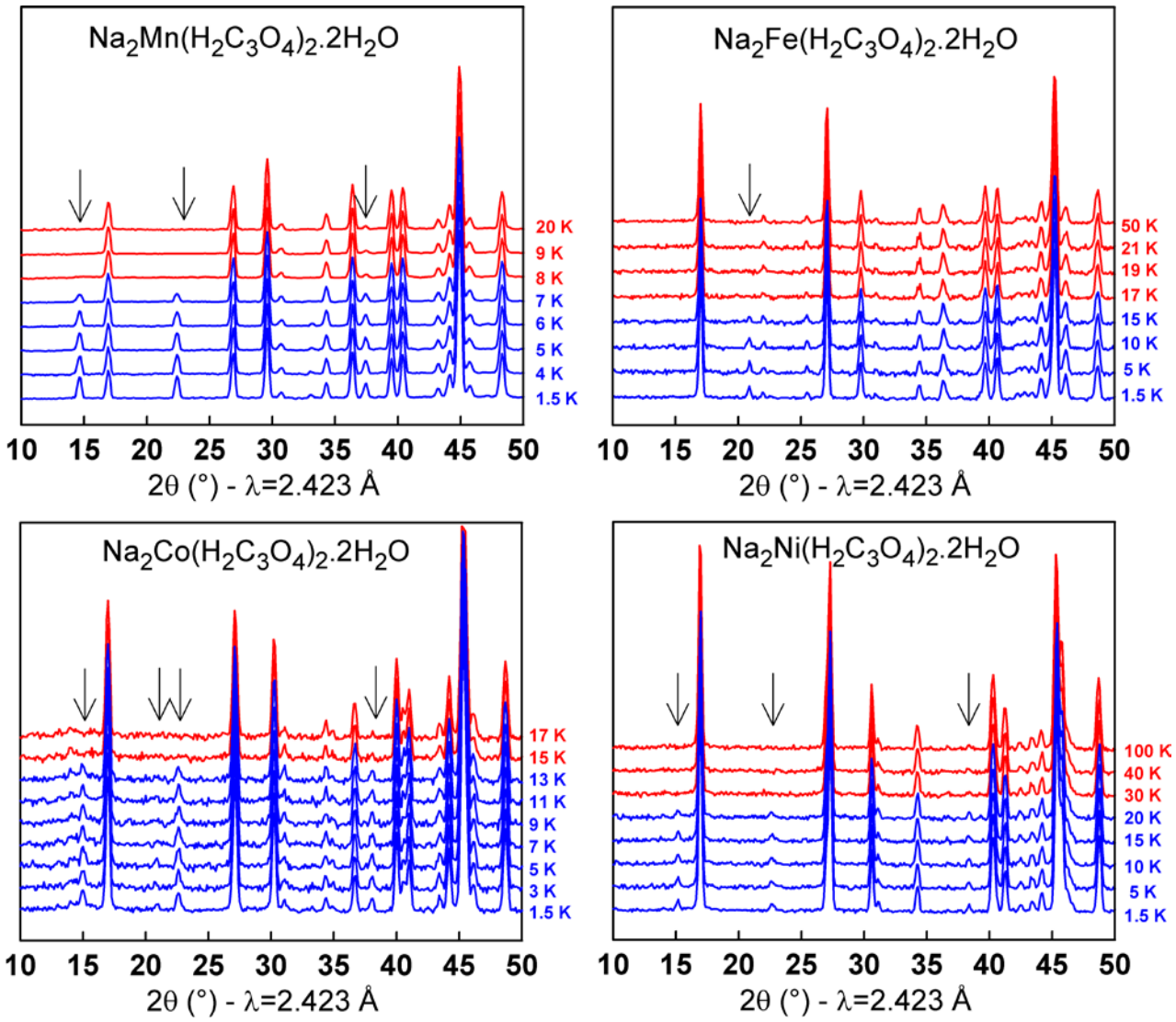
Na2Mn(H2C3O4)2.2H2O
20 K
9 K
8 K
7 K
6 K
5 K
4 K
1.5 K
Na2Fe(H2C3O4)2.2H2O
50 K
21 K
19 K
17 K
15 K
10 K
5 K
1.5 K
Na2Co(H2C3O4)2.2H2O
17 K
15 K
13 K
11 K
9 K
7 K
5 K
3 K
1.5 K
Na2Ni(H2C3O4)2.2H2O
100 K
40 K
30 K
20 K
15 K
10 K
5 K
1.5 K
10 15 20 25 30 35 40 45 50
2θ (°) - λ=2.423 Å

Figure 8

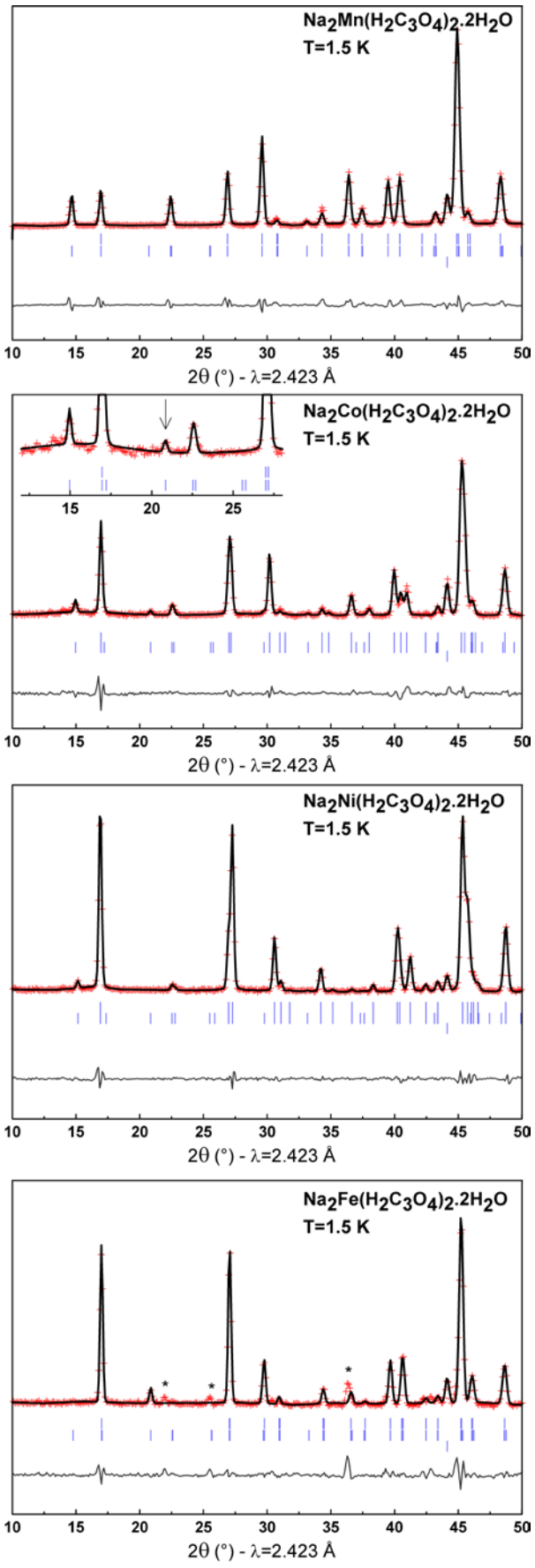
Na2Mn(H2C3O4)2.2H2O
T=1.5 K
2θ (°) - λ=2.423 Å
Na2Co(H2C3O4)2.2H2O
T=1.5 K
2θ (°) - λ=2.423 Å
Na2Ni(H2C3O4)2.2H2O
T=1.5 K
2θ (°) - λ=2.423 Å
Na2Fe(H2C3O4)2.2H2O
T=1.5 K
2θ (°) - λ=2.423 Å

Figure 9

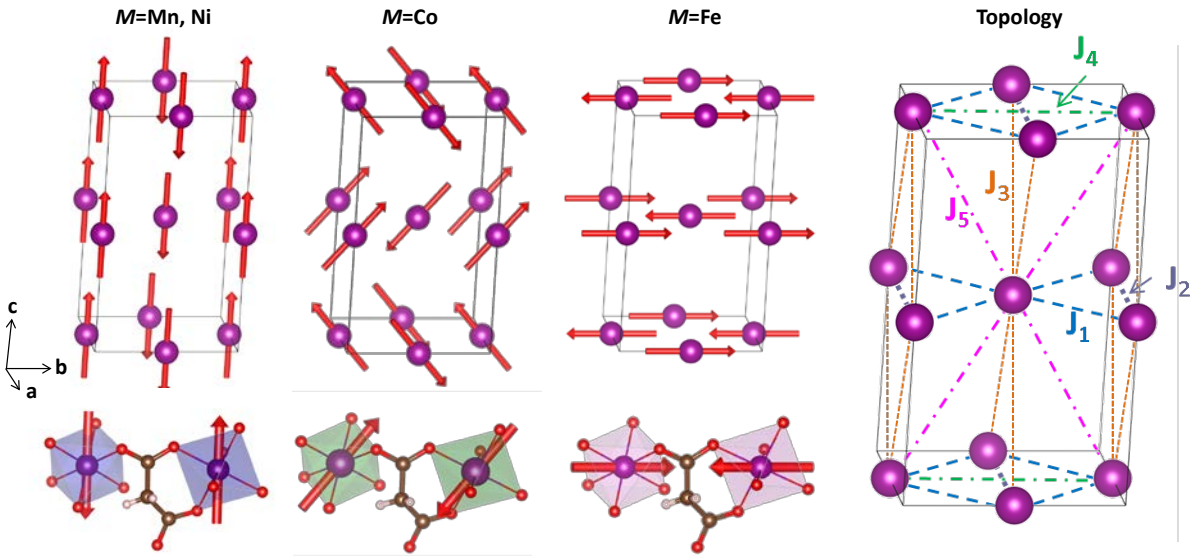

Figure 10

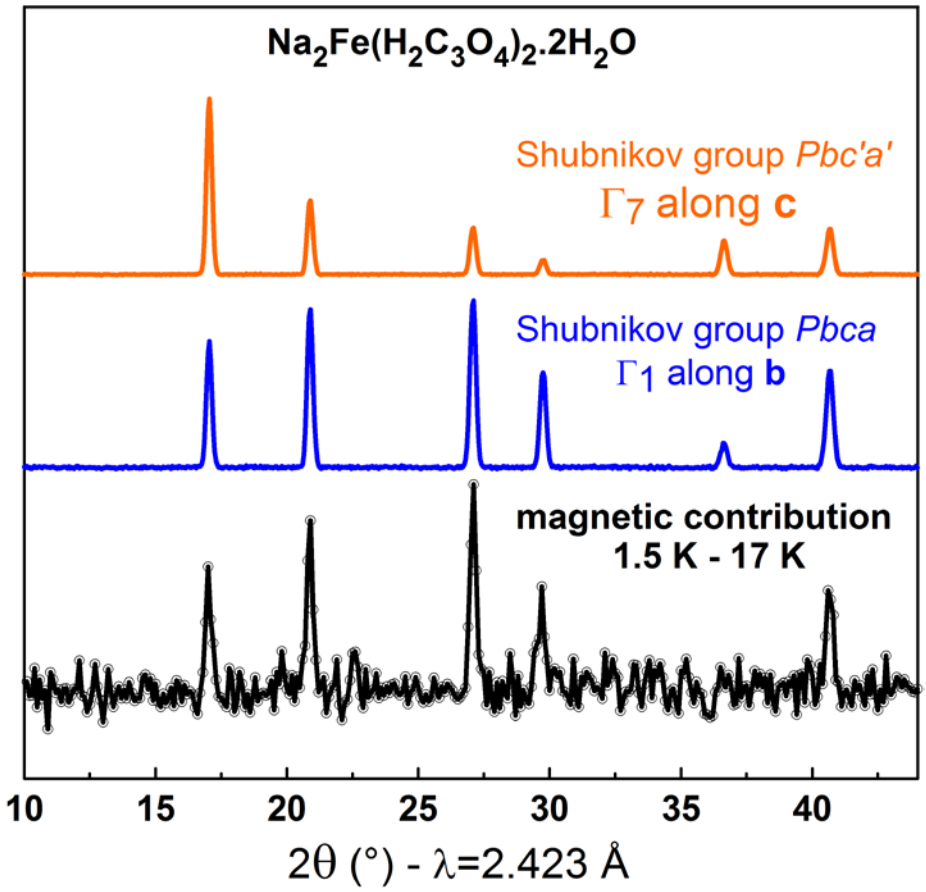
Na2Fe(H2C3O4)2.2H2O
Shubnikov group Pbc'a'
Γ7 along c
Shubnikov group Pbca
Γ1 along b
magnetic contribution
1.5 K - 17 K
10
15
20
25
30
35
40
2θ (°) - λ=2.423 Å

Figure 11

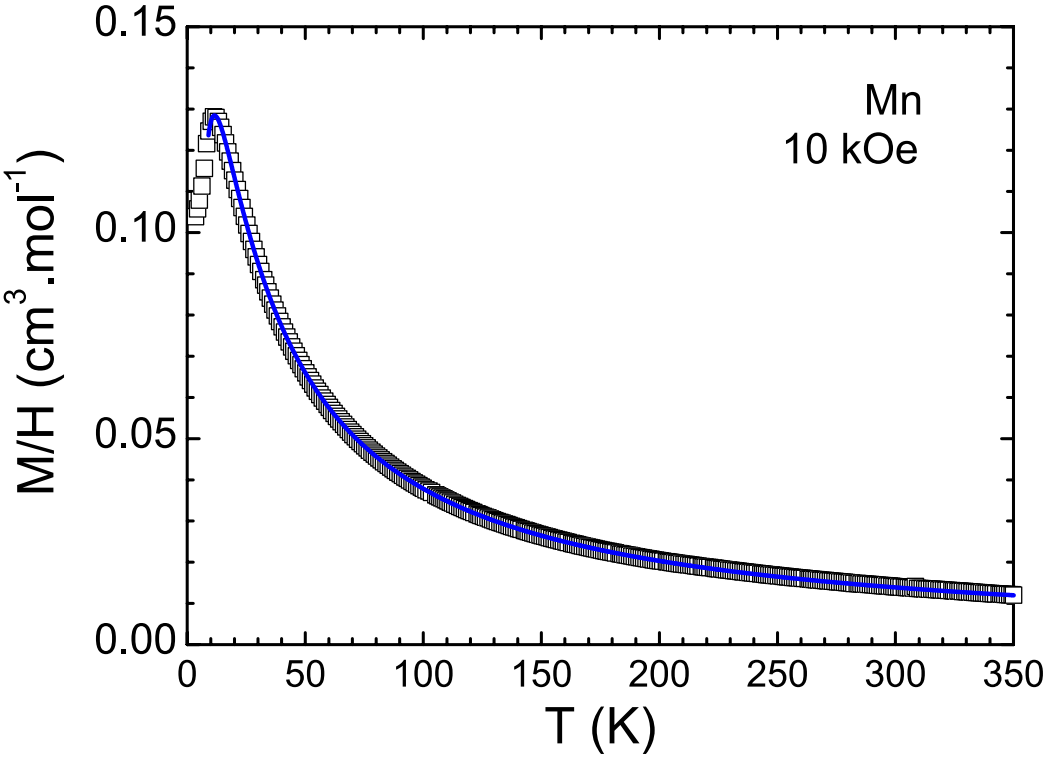
Mn
10 kOe
M/H (cm3.mol-1)
T (K)
0.15
0.10
0.05
0.00
0
50
100
150
200
250
300
350

Table of contents entry:

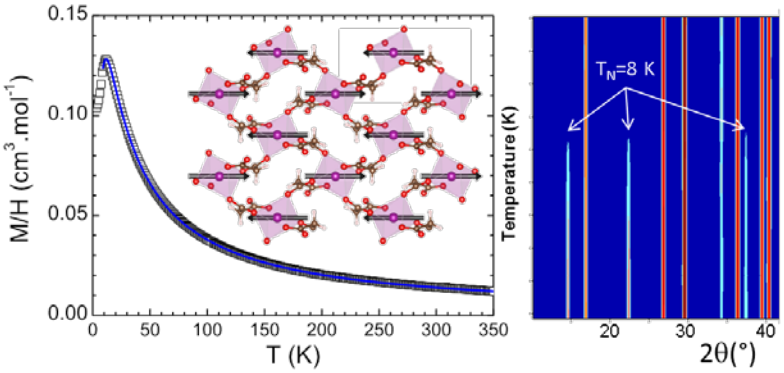

Newly synthetized metal malonates of formula $Na_2M(H_2C_3O_4)_2{\cdot}2H_2O$ (*M*=Mn, Fe, Co, Ni) exhibit distinct long-range antiferromagnetic orders despite their similar structure and chemistry.